Nuclear Science and Techniques (2023) 34:141
https://doi.org/10.1007/s41365-023-01298-w

Calculation of microscopic nuclear level densities based on covariant density functional theory

Kun-Peng Geng[1] · Peng-Xiang Du[1] · Jian Li[1] · Dong-Liang Fang[2]

Received: 24 May 2023 / Revised: 17 July 2023 / Accepted: 29 July 2023 / Published online: 25 September 2023

Abstract
In this study, a microscopic method for calculating the nuclear level density (NLD) based on the covariant density functional theory (CDFT) is developed. The particle-hole state density is calculated by a combinatorial method using single-particle level schemes obtained from the CDFT, and the level densities are then obtained by considering collective effects such as vibration and rotation. Our results are compared with those of other NLD models, including phenomenological, microstatistical and nonrelativistic Hartree–Fock–Bogoliubov combinatorial models. This comparison suggests that the general trends among these models are essentially the same, except for some deviations among the different NLD models. In addition, the NLDs obtained using the CDFT combinatorial method with normalization are compared with experimental data, including the observed cumulative number of levels at low excitation energies and the measured NLDs. The CDFT combinatorial method yields results that are in reasonable agreement with the existing experimental data.

Keywords Nuclear level density · Covariant density functional theory · Combinatorial method

1 Introduction

Nuclear level density (NLD) is the basic physical input for nuclear reactions. This is the key component for the calculation of reaction cross sections relevant to nucleosynthesis [1–6]. The study of NLDs dates back to the 1930s, with Bethe's pioneering work [7]. Since then, many theoretical models such as the back-shifted Fermi gas model (BFM) [8], composite constant temperature model (CTM) [9] and generalized superfluid model (GSM) [10] have been adopted for NLD studies. These phenomenological models are widely used for nuclear reaction calculations. Phenomenological models rely on experimental data for adjusting the parameters; however, experimental data are limited, especially for nuclei far from the β-stability line [11]. To address these difficulties, many microscopic methods have been developed.

Over the past decades, various microscopic approaches for NLD have been proposed, including the equidistant spacing model [12–15], the shell-model Monte Carlo method [16–20], the spectral distribution calculation [21–23], the independent particle model at finite temperature [24–27], the microstatistical methods [28–31] and the random matrix method [32]. Recently, a stochastic estimation method for the level density within the framework of the configuration-interaction shell model (CISM) was proposed [33] and applied in the calculation of NLDs of fission products $^{133-137}$Xe and $^{135-138}$Ba [34]. Over the past two decades, microscopic methods based on the Hartree–Fock–Bogoliubov (HFB) combinatorial model [11] have been developed. The idea of using a combinatorial method to calculate the level densities was derived from the calculation of excitation-state densities [35]. After successfully describing the excitation-state densities using combinations of nucleons occupying single-particle levels at the mean field, it was natural to further describe the level densities by considering

This work was supported by the Natural Science Foundation of Jilin Province (No. 20220101017JC), National Natural Science Foundation of China (No. 11675063), and Key Laboratory of Nuclear Data Foundation (JCKY2020201C157).

✉ Jian Li
jianli@jlu.edu.cn

Dong-Liang Fang
dlfang@impcas.ac.cn

[1] College of Physics, Jilin University, Changchun 130012, China

[2] Institute of Modern Physics, Chinese Academy of Sciences, Lanzhou 730000, China

the collective effects [36]. This combinatorial approach is on par with statistical methods with respect to reproducing experimental data and can provide energy-, spin-, and parity-dependent NLDs beyond the scope of statistical methods [37]. The nonrelativistic HFB combinatorial methods based on Skyrme and Gogny effective interactions have successfully reproduced NLDs for various nuclei [37, 38] and have been applied to astrophysical reactions. The accuracy of NLD is related to the basic information about the nuclear structure, such as single-particle levels, deformation, and binding energy. In recent years, the covariant (relativistic) density functional theory has attracted considerable attention in the field of nuclear physics owing to its successful description of complex nuclear structures and reaction dynamics [39–45]. For instance, it can satisfactorily reproduce the isotopic shifts in Pb isotopes [46] and can naturally explain the origin of the pseudospin and spin symmetries in the antinucleon spectrum [47], as well as provide a good description of the nuclear magnetic moments [48, 49]. Recently, a microstatistical method based on the CDFT was developed to describe NLDs [50]. The method was applied to the calculation of NLDs of ^{94,96,98}Mo and ^{106,108}Pd as well as the odd-A nuclei at saddle point [51], which were in good agreement with experimental data over the entire energy range of the measured values [50]. While the microstatistical method can only calculate energy-dependent NLDs, the combinatorial method can calculate energy-, spin-, and parity-dependent NLDs. Therefore, it is meaningful to calculate the NLDs using the CDFT combinatorial method.

The theoretical framework and methods are introduced in Sect. 2. The NLDs calculated using the CDFT combinatorial method are compared with other NLD predictions and experimental results in Sect. 3. Finally, the conclusions and future prospects are presented in Sect. 4.

2 Theoretical framework

Covariant density functional theory starts from a Lagrangian, and the corresponding Kohn-Sham equations have the form of a Dirac equation with effective fields S and V derived from this Lagrangian [39, 41, 49, 52]. Specifically, the nucleons in the nucleus are described as Dirac particles moving in the average potential field provided by the meson and photon fields, interacting with each other through the exchange of mesons and photons. The Dirac equation is written as follows:

$$[\boldsymbol{\alpha}\cdot\boldsymbol{p}+\beta(m+S)+V]\psi_i=\varepsilon_i\psi_i, \tag{1}$$

where ε_i is the single-particle energy required to calculate the NLDs, and S and V are the relativistic scalar field and time-like component of the vector field, respectively.

Upon obtaining the energy ε, spin projection m, and parity p of the single-particle levels using CDFT, the level information is substituted into the generating function defined in the combinatorial method [11] to obtain the particle-hole state density ρ_i; the generating function $\mathcal{Z}$ is expressed as follows:

$$\mathcal{Z}(x_1,x_2,x_3,x_4)=\prod_{k=1}^{4}\prod_{i=1}^{I_k}(1+x_k p_i^k y^{\varepsilon_i^k} t^{m_i^k}). \tag{2}$$

The above generating function is a straightforward generalization of the function used previously [15] that accounts for not only the energy ε_i^k but also the spin projection m_i^k and parity p_i^k. The variables x_k (k = 1,..., 4) enable us to count the number of particles and holes, y enables us monitor the excitation energies and t of the spin projections, and the indices I_1,...,I_4 denote the number of discrete states considered for each set of single-particle and single-hole states. In practice, $I_2 = Z$ and $I_4 = N$ for nuclei with Z protons and N neutrons. $\mathcal{Z}$ can be expanded into powers of x_k as described below:

$$\mathcal{Z}(x_1,x_2,x_3,x_4)=\sum_{\mathcal{N}}\mathcal{F}_{\mathcal{N}}(y,t)\prod_{k=1}^{4}x_k^{N_k}. \tag{3}$$

The symbol $\mathcal{N}$ denotes any integer combination (N_1, N_2, N_3, N_4). The function $\mathcal{F}(y,t)$ can be expanded into powers of y and t as follows:

$$\mathcal{F}_{\mathcal{N}}(y,t)=\sum_{U}\sum_{M}\sum_{P=-1,+1}C_{\mathcal{N}}(U,M,P)y^U t^M, \tag{4}$$

where U, M, and P denote the excitation energy, spin projection, and parity, respectively. The coefficients $C_{\mathcal{N}}(U,M,P)$ represent the number of solutions. Using the coefficients $C_{\mathcal{N}}(U,M,P)$, the simplest definition of the particle-hole state density ρ_i is obtained as follows:

$$\rho_i(U,M,P)=\frac{1}{\varepsilon_0}C_{\mathcal{N}}(U,M,P). \tag{5}$$

However, the state density ρ_i is strongly dependent on the unit energy ε_0. Therefore, another method suggested by Williams [53] is employed in this study to limit the discretization effects, as explained below.

Summing all the $C_{\mathcal{N}}$ values up to a given excitation energy U, we first obtain the cumulative number of states $N_{\mathcal{N}}(U,M,P)$, which represents the number of particle-hole states with excitation energy E such that $0 \le E < U$. The particle-hole state density is defined as follows:

$$\rho_i=\frac{dN_{\mathcal{N}}(U,M,P)}{dU}. \tag{6}$$

The calculated particle-hole state density ρ_i is related only to the particle-hole excitation. Two special collective effects must be considered to obtain the level density, namely

rotational and vibrational effects. If the nucleus under consideration displays spherical symmetry, the intrinsic and laboratory frames coincide, and the level density is trivially obtained using the following relation [7]:

$$\rho_{\rm sph}(U,M,P) = \rho_i(U,M=J,P) - \rho_i(U,M=J+1,P). \quad (7)$$

For deformed nuclei, within the hypothesis of axial symmetry, the NLD, after accounting for the rotational effect, is expressed as follows:

$$\begin{aligned}\rho_{\rm def}(U,M,P) = \frac{1}{2}\Bigg[\sum_{K=-J,K\neq 0}^{J}\rho_i(U-E_{\rm rot}^{J,K},K,P)\Bigg] \\ +(\delta_{(J{\rm even})}\delta_{(p=+)}\rho_i(U-E_{\rm rot}^{J,K},0,P) \\ +\delta_{(J{\rm odd})}\delta_{(p=-)}\rho_i(U-E_{\rm rot}^{J,K},0,P)).\end{aligned} \quad (8)$$

The fraction 1/2 accounts for the fact that in mirror axially symmetric nuclei, the intrinsic states with spin projections $+K$ and $-K$ yield the same rotational levels. Moreover, in the second term of the summation, the symbol $\delta_{(x)}$ (defined by $\delta_{(x)} = 1$ if x holds true and 0 otherwise) restricts the rotational bands built on intrinsic states with spin projection $K = 0$ and parity P to level sequences 0, 2, 4,... for $P = +$ and 1, 3, 5,... for $P = -$. Finally, the rotational energy is obtained using the following expression [54]:

$$E_{\rm rot}^{J,K} = \frac{J(J+1)-K^2}{2\mathcal{J}_\perp}, \quad (9)$$

where $\mathcal{J}_\perp$ denotes the moment of inertia of a nucleus rotating around the axis perpendicular to the symmetry axis. In this study, $\mathcal{J}_\perp$ is approximated by the rigid-body value $\mathcal{J}_\perp^{\rm rigid}$, which is expressed as follows:

$$\mathcal{J}_\perp^{\rm rigid} = \frac{2}{5}mR^2\left(1+\sqrt{\frac{5}{16\pi}}\beta^2\right) \quad (10)$$

for an ellipsoidal shape with the quadrupole deformation parameter β. The vibration enhancement is approximated as [55]:

$$K_{\rm vib} = \exp[\delta S - (\delta U/T)], \quad (11)$$

where S denotes entropy, U denotes the excitation energy, and T denotes the nuclear temperature.

Finally, a phenomenological damping function is introduced to avoid sharp transitions between the spherical and deformed level densities that affect the NLD predictions. The expression for the NLD after introduction of the damping function is [31]:

$$\begin{aligned}\rho(U,M,P) = [1-f_{\rm dam}(U)]K_{\rm vib}\rho_{\rm sph}(U,M,P) \\ +f_{\rm dam}(U)K_{\rm vib}\rho_{\rm def}(U,M,P).\end{aligned} \quad (12)$$

The damping function $f_{\rm dam}$ is expressed as follows [38]:

$$f_{\rm dam} = 1 - \frac{1}{1+\exp(\beta-0.18)/0.038}, \quad (13)$$

where β is the quadrupole deformation parameter. Parameters 0.18 and 0.038 are adjusted according to the experimental data at the neutron separation energy S_n [56]. The expression for $f_{\rm dam}$ developed previously [38] was simplified to depend only on the nuclear deformation, thereby reducing the number of phenomenological parameters. This damping function is used to suppress the discontinuities that occur between the spherical and deformed NLDs and ensure a smooth change of shape from deformed to spherical.

3 Results and discussion

In this section, we present our results for the NLDs obtained using the combinatorial method based on the CDFT and compare them with the results obtained using other NLD models [57] and experimental data [58, 59]. The effective meson-exchange interaction parameter PK1 [60] is adopted throughout the CDFT calculations. For spherical CDFT calculations, we fixed the box size as $R_{\rm box} = 20$ fm and the step size as $\Delta r = 0.1$ fm. In the present deformed CDFT calculations, the Dirac equation for nucleons and the Klein–Gordon equations for mesons are solved using an isotropic harmonic oscillator, and a basis for the 18 major oscillator shells is adopted.

The combinatorial results rely on the properties of single-particle levels. To understand the effect of using different effective interactions on the NLDs, the NLDs of ^{112}Cd and ^{162}Dy obtained with different CDFT effective interactions, namely PK1 [60], NL3 [61], DD-ME2 [62], and DD-PC1 [63] are presented for comparison in Fig. 1. For nuclei with small deformations (^{112}Cd), the NLDs for the four effective

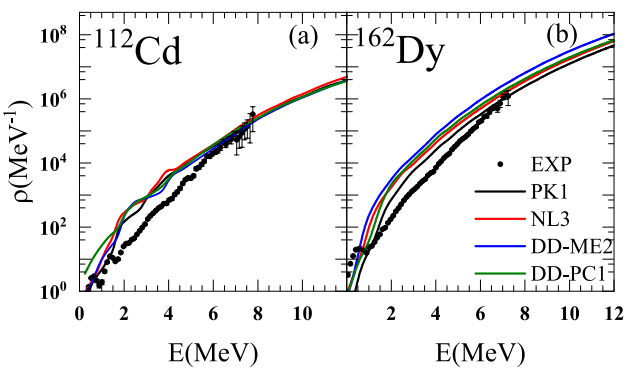

Fig. 1 (Color online) Comparison of NLDs calculated using different effective interactions under CDFT with experimental data [58, 59]

interactions are close for excitation energies above 4 MeV. However, significant differences are observed for excitation energies below 4 MeV. This difference arises from the fact that the single-particle energies near the Fermi level are exceptionally sensitive to the choice of effective interaction, especially when the Fermi level is near the proton or neutron shells. Meanwhile, the CDFT calculations with the chosen interactions do not adequately reproduce the single-particle levels of the magic nuclei ^{132}Sn [64], which explains the deviations of our results from the measurements presented in Fig. 1. For the well-deformed ^{162}Dy, the NLDs calculated with the four effective interactions deviate from each other in the entire region of the excitation energy, although the overall trend is consistent. This deviation at low excitation energies is mainly caused by differences in the single-particle energies around the Fermi level. Meanwhile, the entropy S obtained from the four effective interactions is significantly different for nuclei with large deformations, which ultimately leads to deviation of the NLDs at high excitation energies. Compared with the experimental data of ^{112}Cd [58] and ^{162}Dy [59] extracted by the Oslo group based on the analysis of particle-γ coincidence in the (^{3}He, $\alpha\gamma$) and (^{3}He, ^{3}He" γ) reactions, the deviation between the NLDs obtained by using PK1 effective interaction and the results obtained by using other effective interactions is within a reasonable range.

The nonrelativistic HFB combinatorial methods, including Skyrme and Gogny interactions, have been widely used in NLD predictions [55, 58]; the NLDs of spherical nuclei (^{55}Co, ^{132}Sn, and ^{208}Pb) and deformed nuclei (^{94}Mo, ^{95}Mo, and ^{166}Er) calculated using the CDFT combinatorial method are compared with the corresponding experimental data, as illustrated in Fig. 2.

For ^{55}Co, the CDFT combinatorial method yields a lower NLD than the experimental value, whereas the Skyrme combinatorial method yields a higher NLD. Although the results of the Gogny combinatorial method are closer to the experimental data to a certain extent, a strong oscillation exists. For ^{132}Sn and ^{208}Pb, the results of the CDFT combinatorial method are similar to those of the Skyrme combinatorial method; however, the results of the Gogny combinatorial method are significantly lower than those of the two methods. Compared to the experimental data, the CDFT combinatorial method can better describe the NLD of ^{208}Pb. The NLDs of ^{55}Co, ^{132}Sn, and ^{208}Pb obtained using the three combinatorial methods are oscillatory to a certain extent because the three nuclei are spherical with highly degenerate single-particle levels with a strong shell effect.

For ^{94}Mo, the results of both the CDFT and Skyrme combinatorial methods are closer to the experimental data than those of the Gogny combinatorial method. For ^{95}Mo and ^{166}Er, the NLDs obtained using the three combinatorial methods are similar and slightly higher than

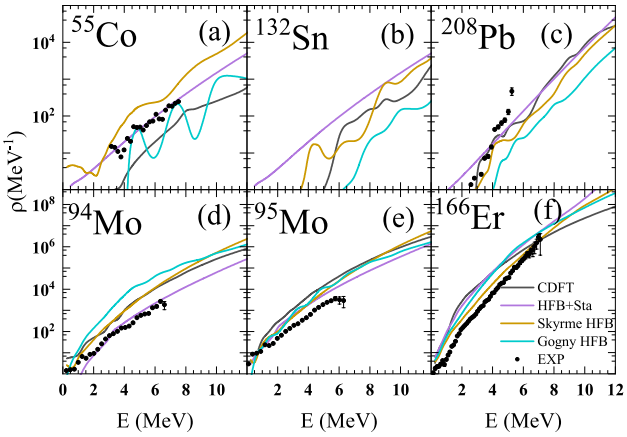

Fig. 2 (Color online) Comparison of NLDs calculated based on the CDFT combinatorial method with results from the HFB combinatorial methods and microstatistical method (HFB+Sta) [31, 37, 38]. The experimental data are taken from Refs. [65–68]

the experimental data. It should be emphasized that the deformed nuclei ^{94}Mo, ^{95}Mo, and ^{166}Er break the single-particle level degeneracy, yielding smoother NLDs, as shown in Fig. 2. It is noteworthy that the CDFT combinatorial method yields higher NLDs for ^{94}Mo and ^{95}Mo. One possible reason for this is that the CDFT combinatorial method uses a rigid-body value when considering the rotational effect, which is inappropriate for soft nuclei [69].

In addition, the NLDs of ^{55}Co and ^{94}Mo can be adequately described by the microstatistical model [31] relative to the CDFT combinatorial method, while both models provide similar descriptions for the NLDs of ^{95}Mo and ^{166}Er. In comparison, the microstatistical model yields relatively smooth results for spherical and deformed nuclei, which do not satisfactorily reflect the shell effect. Therefore, it can be concluded that the CDFT combinatorial method is as capable of describing NLDs as the other two combinatorial methods and the microstatistical model.

Furthermore, it is necessary to compare the NLDs obtained in the study with those obtained using phenomenological models (BFM, CTM, and GSM) [57]. Phenomenological models can adequately describe the experimental data at neutron separation by fitting the experimental data. The level densities at the neutron separation energy are the most commonly used experimental data and are obtained using the mean distance D_0 of the s-wave resonance. The NLDs of the even-even nuclei (^{112}Cd and ^{162}Dy), odd-A nuclei (^{51}V, ^{97}Mo, and ^{119}Sn), and odd-odd nucleus (^{60}Co) calculated using the CDFT combinatorial method are compared with those obtained using phenomenological models and the available experimental data, as demonstrated in Fig. 3. As shown in Fig. 3, the CDFT combinatorial method is as capable of reproducing the experimental data on the neutron separation energy as the phenomenological

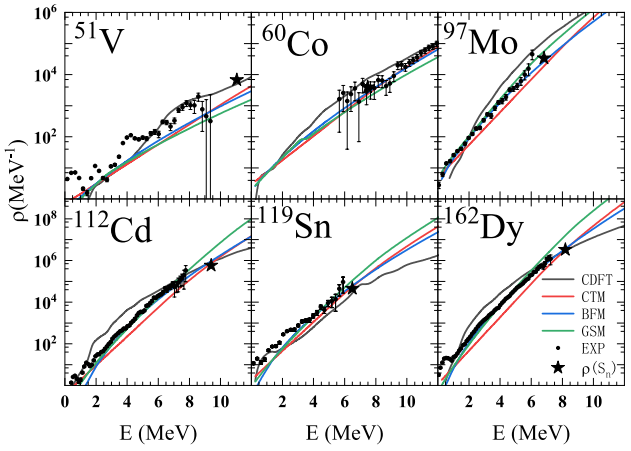

Fig. 3 (Color online) Comparison of NLDs obtained from the CDFT combinatorial method with other NLD predictions [57] and experimental data [58, 58, 59, 59, 66, 70]. The full asterisk corresponds to the experimental data at the neutron separation energy S_n [56]

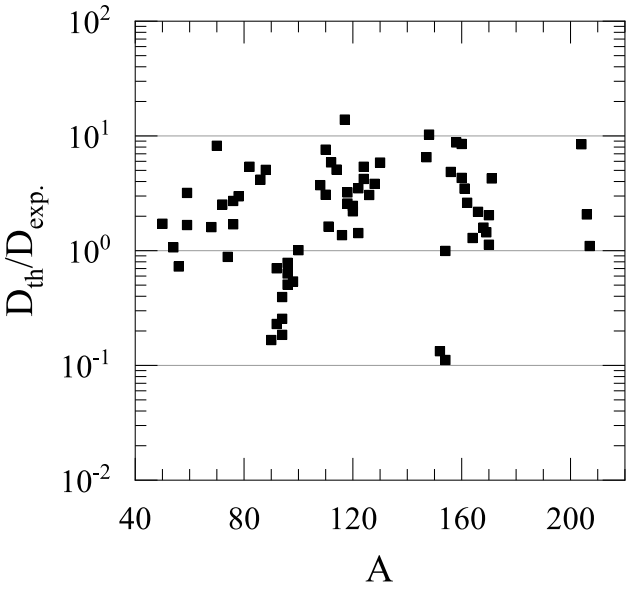

Fig. 4 Ratio of the s-wave neutron resonance spacing for the CDFT combinatorial method (D_{th}) and the experimental data ($D_{\text{exp.}}$), as compiled in Ref. [56]

models; in particular, the CDFT combinatorial method can adequately describe the NLD of ^{51}V. In addition, the overall description of the experimental data below the neutron separation energy provided by the CDFT combinatorial method is similar to that of the phenomenological methods. In conclusion, although there are few differences in the results for each NLD model, the overall ability to describe the experimental data is similar.

The most extensive and reliable sources of experimental information on NLD are the s-wave neutron resonance spacing D_0 [56] and observed low-energy excited levels [56]. To measure the dispersion between the theoretical and experimental D_0, the f_{rms} factor is defined as follows:

$$f_{\text{rms}} = \exp\left[\frac{1}{N_e}\sum_{i=1}^{N_e}\ln^2\frac{\mathrm{D}^{\mathrm{i}}_{\mathrm{th}}}{\mathrm{D}^{\mathrm{i}}_{\mathrm{exp.}}}\right]^{1/2}, \tag{14}$$

where $D_{\text{th}}(D_{\text{exp.}})$ is the theoretical (experimental) resonance spacing, and N_e is the number of nuclei in the compilation. The results for the ratio of D_{th} to $D_{\text{exp.}}$ are presented in Fig. 4. Upon calculation, we find that $f_{\text{rms}} = 3.62$, with a total of 66 nuclei. Under the same calculation conditions, f_{rms} of the Gogny (D1S) interaction based on the HFB combinatorial method is measured as 7.25 [11]. At present, the result of the CDFT combinatorial method is larger than the $f_{\text{rms}} = 1.8$ deviation of the phenomenological BFM [10] and the $f_{\text{rms}} = 2.1$ value obtained using the microstatistical method [31]. However, the HFB combinatorial method based on the Skyrme effective interaction improves the pairing correlation [55] and collective effects, yielding the value $f_{\text{rms}} = 2.3$ [37]. Future studies can extend the same approach to improve the CDFT combinatorial method.

When phenomenological NLDs are used in nuclear physics applications, such as nuclear data evaluation or accurate and reliable estimation of reaction cross-sections, a few parameters are used considering the dependence of the phenomenological expressions [71]. The results of the combinatorial method can also normalize both the experimental-level scheme at a low excitation energy and the neutron resonance spacing at $U = S_n$ in a manner similar to what is typically used for analytical formulas. More precisely, the normalized level density can be obtained as follows: [37]

$$\rho(U,J,P) = e^{\alpha\sqrt{U-\delta}} \times \rho(U-\delta,J,P), \tag{15}$$

where the energy shift δ is extracted from the analysis of the cumulative number of levels and α can be obtained using the following expression:

$$\rho_{\text{th}}(S_n) \times e^{\alpha\sqrt{S_n}} = \rho_{\text{exp.}}(S_n). \tag{16}$$

With this normalization, the experimental low-lying states and D_0 values can be reproduced reasonably well.

As an illustration, the variation in the NLDs obtained using the CDFT combinatorial method before and after normalization is shown in Fig. 5. When normalization is applied, the NLDs pass through the experimental data at the neutron separation energy S_n. As shown in Fig. 5a, if the theoretically calculated value is close to the experimental value at the neutron separation energy S_n, the results before and after normalization do not change

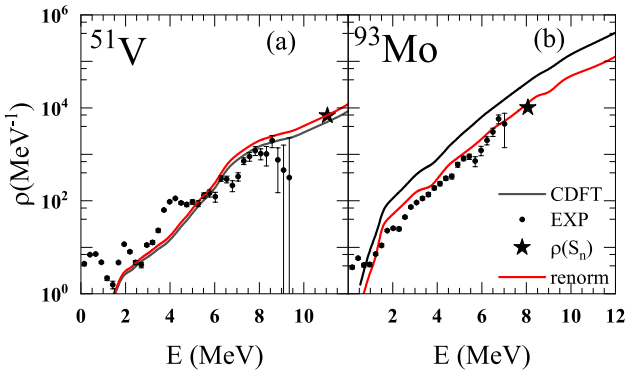

Fig. 5 (Color online) NLDs obtained using the CDFT combinatorial method with (red) and without (black) normalization. The experimental data are taken from Refs. [56, 66, 70]

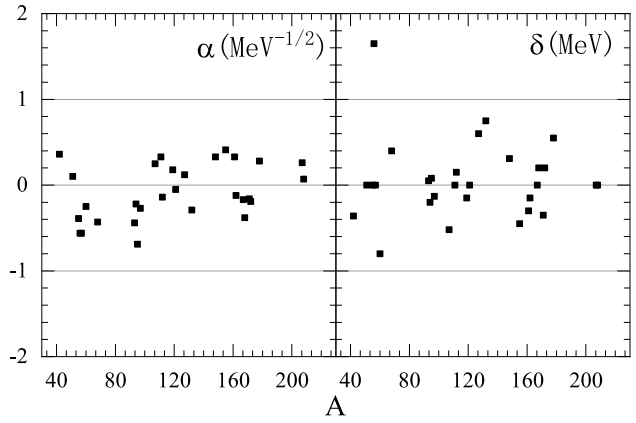

Fig. 6 Normalized parameters α (left) and δ (right) are plotted as functions of the atomic mass number

significantly. As shown in Fig. 5b, the results after normalization are in better agreement with the experimental data [70], particularly above 2 MeV. This is because the coefficient $e^{\alpha\sqrt{U-\delta}}$ is related to the excitation energy U, and when U is small, normalization has a negligible effect. α and δ values of some nuclei are presented in Fig. 6.

Finally, the NLDs calculated using the CDFT combinatorial method are compared with the observed low-energy excited levels, which constitute the most extensive and reliable source

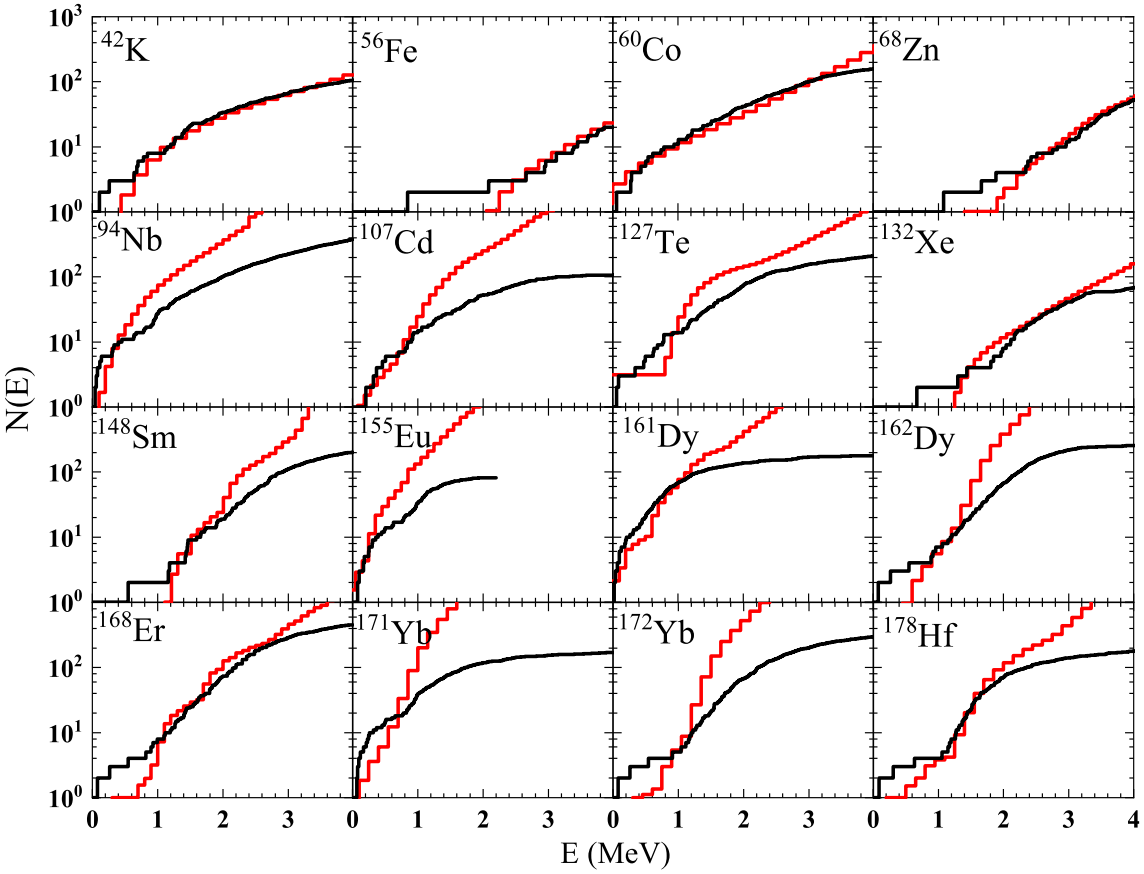

Fig. 7 (Color online) Comparison of the results obtained from the CDFT combinatorial method (red lines) with the cumulative number of observed levels [56] (black lines) as a function of the excitation energy

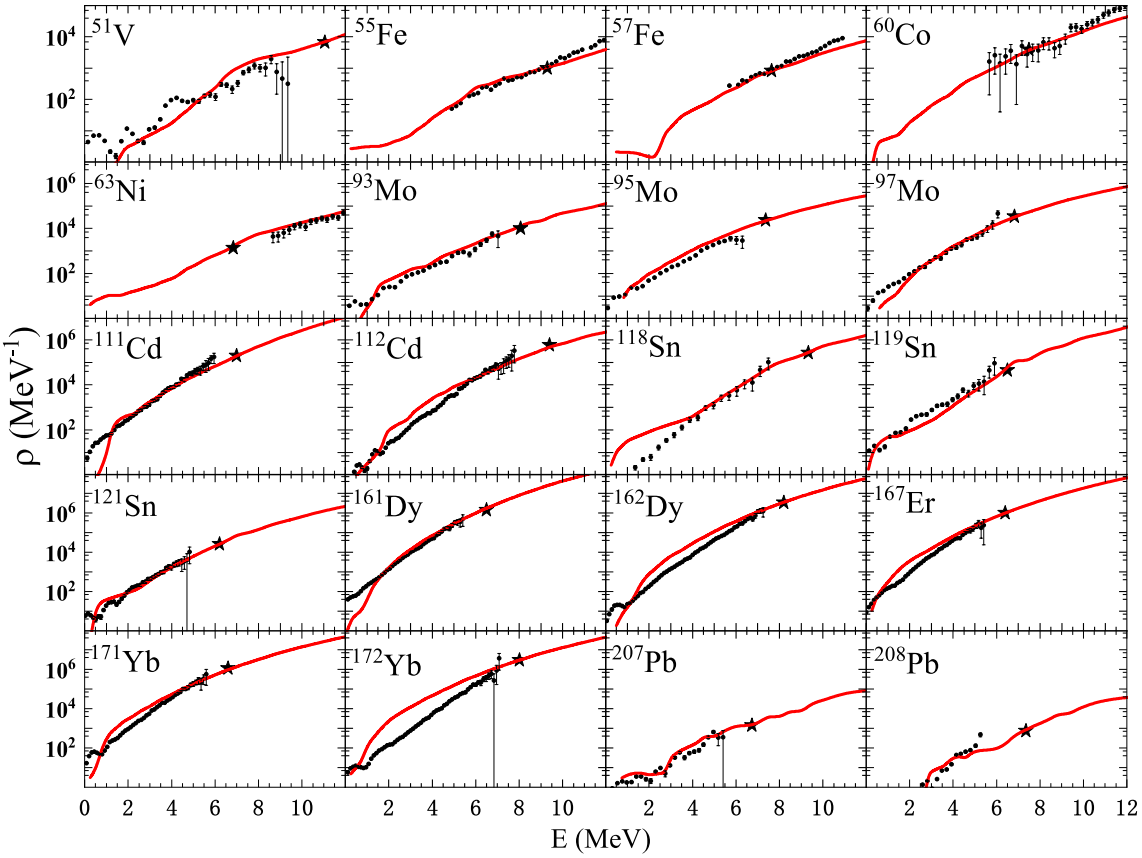

Fig. 8 (Color online) Comparison between the calculated NLDs based on the CDFT combinatorial method (red lines) and experimental data [58, 59, 66–68, 70, 72–75] (black dot). The full asterisk corresponds to the experimental data at the neutron separation energy S_n [56]

of experimental information on NLDs [56]. The cumulative number of nuclear levels $N(U)$ indicates the sum of the number of levels below the excitation energy U (including U)

$$N(U) = \sum_{M}\sum_{P} N(U, M, P). \tag{17}$$

Here, $N(U, M, P)$ is the cumulative number of levels under spin M and parity P at the excitation energy E. The predicted cumulative number of levels $N(U)$ is compared with the experimental value [56], as shown in Fig. 7, and the results include both light and heavy nuclei, as well as spherical and deformed nuclei. Overall, the results of the CDFT combinatorial method are in reasonable agreement with the experimental data at lower excitation energies, especially for light nuclei. At high excitation energies, the theoretically calculated cumulative number of nuclear levels is higher than the experimental value. The NLDs increase rapidly with increasing excitation energy, and $N(U)$ is expected to gradually increase at high excitation energies. However, the experimental levels of the cumulative number gradually stabilize. This may be attributed to the limitations imposed by the experimental conditions owing to which the number of levels cannot be counted completely.

In Fig. 8, the CDFT combinatorial method predictions after normalization are compared with the experimental data extracted using the Oslo method [58, 59, 66–68, 70, 72, 73] and the particle evaporation spectrum [74, 75]. The Oslo method is model-dependent. To extract the absolute value of the total level density from the measured data, the experimental NLDs must be normalized by the total level density at the neutron binding energy, which in turn is derived from the neutron resonance spacing. For a meaningful comparison between the CDFT combinatorial predictions and data obtained using the Oslo method, it is important to normalize the NLDs obtained using the CDFT combinatorial method to the level density value at $U = S_n$ considered by the Oslo group. As shown in Fig. 8, the results of the CDFT combinatorial method after normalization agree well with the experimental data below S_n, except for the small NLDs of ^{111}Cd and ^{161}Dy at low excitation energies. This low result is due to the larger energy spacing of the theoretically calculated single-particle levels near the Fermi level. Overall,

the results obtained using the CDFT combinatorial method are reliable.

4 Summary and prospects

A combinatorial method was adopted to describe the nuclear level densities for nuclear reaction calculations. The particle-hole state density was obtained using a combinatorial method with the single-particle level provided by the PK1 effective interaction based on CDFT. Energy-, spin-, and parity-dependent NLDs were obtained after accounting for collective effects, including vibration and rotation. Our results were compared with those obtained using other NLD models, including phenomenological, microstatistical, and nonrelativistic HFB combinatorial models. The comparison suggests that bar some small deviations among the different NLD models, the general trends among these models are essentially the same. In conclusion, the CDFT combination method can reproduce experimental data at or below the neutron separation energy. This implies that the CDFT combinatorial method is as reliable as the other models at describing NLDs. Finally, the comparison of the NLDs of the CDFT combinatorial method with normalization with the experimental data exhibited excellent agreement between the observed cumulative number of levels at low excitation energies and the measured NLDs below the neutron separation energy.

Our results demonstrate the predictive power of the CDFT combinatorial method. However, in our approach, pairing correlations are not considered and the collective effects are empirical. In our future work, we aim to improve upon the CDFT combinatorial method by considering the inclusion of energy-dependent pairing correlations and adopting a partition function approach to the treatment of vibrational enhancement. These results can potentially help our study of important neutron capture processes, such as the r-process.

Author Contributions All authors contributed to the study conception and design. Material preparation, data collection and analysis were performed by Kun-Peng Geng, Peng-Xiang Du, Jian Li and Dong-Liang Fang. The first draft of the manuscript was written by Kun-Peng Geng and Peng-Xiang Du, and all authors commented on previous versions of the manuscript. All authors read and approved the final manuscript.

Data availability The data that support the findings of this study are openly available in Science Data Bank at https://www.doi.org/10.57760/sciencedb.j00186.00211 and https://cstr.cn/10.57760/sciencedb.j00186.00211.

Declarations

Conflict of interest The authors declare that they have no conflict of interest.

References

1. H.A. Bethe, R.F. Bacher, Nuclear physics A. Stationary states of nuclei. Rev. Mod. Phys. **8**, 82–229 (1936). https://doi.org/10.1103/RevModPhys.8.82
2. P. Möller, A. Sierk, T. Ichikawa et al., Nuclear ground-state masses and deformations: Frdm (2012). At. Data Nucl. Data Tables **109–110**, 1–204 (2016). https://doi.org/10.1016/j.adt.2015.10.002
3. H.A. Bethe, Nuclear physics B. Nuclear dynamics, theoretical. Rev. Mod. Phys. **9**, 69–244 (1937). https://doi.org/10.1103/RevModPhys.9.69
4. C. Yalcin, The cross-section calculation of ^{112}Sn(α,γ)^{116}Te reaction with different nuclear models at the astrophysical energy range. Nucl. Sci. Tech **28**, 113 (2017). https://doi.org/10.1007/s41365-017-0267-y
5. J.H. Luo, J.C. Liang, L. Jiang et al., Measurement of ^{134}xe(n,2n)^{133m,g}xe reaction cross sections in 14-mev region with detailed uncertainty quantification. Nucl. Sci. Tech. **34**, 4 (2023). https://doi.org/10.1007/s41365-022-01158-z
6. P.H. Chen, H. Wu, Z.X. Yang et al., Prediction of synthesis cross sections of new moscovium isotopes in fusion-evaporation reactions. Nucl. Sci. Tech. **34**, 7 (2023). https://doi.org/10.1007/s41365-022-01157-0
7. H.A. Bethe, An attempt to calculate the number of energy levels of a heavy nucleus. Phys. Rev. **50**, 332–341 (1936). https://doi.org/10.1103/PhysRev.50.332
8. W. Dilg, W. Schantl, H. Vonach et al., Level density parameters for the back-shifted Fermi gas model in the mass range $40 < A < 250$. Nucl. Phys. A **217**, 269–298 (1973). https://doi.org/10.1016/0375-9474(73)90196-6
9. A. Gilbert, A.G.W. Cameron, A composite nuclear-level density formula with shell corrections. Can. J. Phys. **43**, 1446–1496 (1965). https://doi.org/10.1139/p65-139
10. A. Koning, S. Hilaire, S. Goriely, Global and local level density models. Nucl. Phys. A **810**, 13–76 (2008). https://doi.org/10.1016/j.nuclphysa.2008.06.005
11. S. Hilaire, J. Delaroche, M. Girod, Combinatorial nuclear level densities based on the Gogny nucleon–nucleon effective interaction. Eur. Phys. J. A **12**, 169–184 (2001). https://doi.org/10.1007/s100500170025
12. F.C. Williams, Particle-hole state density in the uniform spacing model. Nucl. Phys. A **166**, 231–240 (1971). https://doi.org/10.1016/0375-9474(71)90426-X
13. E. Běták, J. Dobeš, The finite depth of the nuclear potential well in the exciton model of preequilibrium decay. Z. Phys. A **279**, 319–324 (1976). https://doi.org/10.1007/BF01408305
14. P. Obložinský, Particle-hole state densities for statistical multistep compound reactions. Nucl. Phys. A **453**, 127–140 (1986). https://doi.org/10.1016/0375-9474(86)90033-3
15. S. Hilaire, J. Delaroche, A. Koning, Generalized particle-hole state densities within the equidistant spacing model. Nucl. Phys. A **632**, 417–441 (1998). https://doi.org/10.1016/S0375-9474(98)00003-7
16. Y. Alhassid, S. Liu, H. Nakada, Particle-number reprojection in the shell model Monte Carlo method: application to nuclear level densities. Phys. Rev. Lett. **83**, 4265–4268 (1999). https://doi.org/10.1103/PhysRevLett.83.4265
17. W.E. Ormand, Estimating the nuclear level density with the Monte Carlo shell model. Phys. Rev. C **56**, R1678–R1682 (1997). https://doi.org/10.1103/PhysRevC.56.R1678
18. J.A. White, S.E. Koonin, D.J. Dean, Shell model Monte Carlo investigation of rare earth nuclei. Phys. Rev. C **61**, 034303 (2000). https://doi.org/10.1103/PhysRevC.61.034303

19. N. Cerf, Combinatorial nuclear level density by a Monte Carlo method. Phys. Rev. C **49**, 852–866 (1994). https://doi.org/10.1103/PhysRevC.49.852
20. N. Cerf, Realistic microscopic level densities for spherical nuclei. Phys. Rev. C **50**, 836–844 (1994). https://doi.org/10.1103/PhysRevC.50.836
21. B. Strohmaier, S.M. Grimes, H. Satyanarayana, Spectral distribution calculations of the level density of ^{24}Mg. Phys. Rev. C **36**, 1604–1610 (1987). https://doi.org/10.1103/PhysRevC.36.1604
22. S.M. Grimes, T.N. Massey, New expansion technique for spectral distribution calculations. Phys. Rev. C **51**, 606–610 (1995). https://doi.org/10.1103/PhysRevC.51.606
23. J.B. French, K.F. Ratcliff, Spectral distributions in nuclei. Phys. Rev. C **3**, 94–117 (1971). https://doi.org/10.1103/PhysRevC.3.94
24. N.D. Dang, N.Q. Hung, L.T.Q. Huong, Testing the constant-temperature approach for the nuclear level density. Phys. Rev. C **96**, 054321 (2017). https://doi.org/10.1103/PhysRevC.96.054321
25. N.Q. Hung, N.D. Dang, L.T.Q. Huong, Simultaneous microscopic description of nuclear level density and radiative strength function. Phys. Rev. Lett. **118**, 022502 (2017). https://doi.org/10.1103/PhysRevLett.118.022502
26. B. Dey, D. Pandit, S. Bhattacharya et al., Level density and thermodynamics in the hot rotating ^{96}Tc nucleus. Phys. Rev. C **96**, 054326 (2017). https://doi.org/10.1103/PhysRevC.96.054326
27. B. Dey, N. Quang Hung, D. Pandit et al., S-shaped heat capacity in an odd–odd deformed nucleus. Phys. Lett. B **789**, 634–638 (2019). https://doi.org/10.1016/j.physletb.2018.12.007
28. B. Agrawal, A. Ansari, Excitation energy and angular momentum dependence of nuclear level densities and spin cut-off factor in spa and spa + rpa approaches. Nucl. Phys. A **640**, 362–374 (1998). https://doi.org/10.1016/S0375-9474(98)00462-X
29. S. Goriely, A new nuclear level density formula including shell and pairing correction in the light of a microscopic model calculation. Nucl. Phys. A **605**, 28–60 (1996). https://doi.org/10.1016/0375-9474(96)00162-5
30. P. Decowski, W. Grochulski, A. Marcinkowski et al., On superconductivity effects in nuclear level density. Nucl. Phys. A **110**, 129–141 (1968). https://doi.org/10.1016/0375-9474(68)90687-8
31. P. Demetriou, S. Goriely, Microscopic nuclear level densities for practical applications. Nucl. Phys. A **695**, 95–108 (2001). https://doi.org/10.1016/S0375-9474(01)01095-8
32. T. Papenbrock, H.A. Weidenmüller, Colloquium: random matrices and chaos in nuclear spectra. Rev. Mod. Phys. **79**, 997–1013 (2007). https://doi.org/10.1103/RevModPhys.79.997
33. N. Shimizu, Y. Utsuno, Y. Futamura et al., Stochastic estimation of nuclear level density in the nuclear shell model: an application to parity-dependent level density in 58ni. Phys. Lett. B **753**, 13–17 (2016). https://doi.org/10.1016/j.physletb.2015.12.005
34. J. Chen, M. Liu, C. Yuan et al., Shell-model-based investigation on level density of xe and ba isotopes. Phys. Rev. C **107**, 054306 (2023). https://doi.org/10.1103/PhysRevC.107.054306
35. J. Berger, M. Martinot, Shell effects on state densities with given numbers of excited protons and neutrons. Nucl. Phys. A **226**, 391–412 (1974). https://doi.org/10.1016/0375-9474(74)90491-6
36. M. Girod, P. Dessagne, M. Bernas et al., Spectroscopy of neutron-rich nickel isotopes: experimental results and microscopic interpretation. Phys. Rev. C **37**, 2600–2612 (1988). https://doi.org/10.1103/PhysRevC.37.2600
37. S. Goriely, S. Hilaire, A.J. Koning, Improved microscopic nuclear level densities within the Hartree–Fock–Bogoliubov plus combinatorial method. Phys. Rev. C **78**, 064307 (2008). https://doi.org/10.1103/PhysRevC.78.064307
38. S. Hilaire, M. Girod, S. Goriely et al., Temperature-dependent combinatorial level densities with the D1M Gogny force. Phys. Rev. C **86**, 064317 (2012). https://doi.org/10.1103/PhysRevC.86.064317
39. P. Ring, Relativistic mean field theory in finite nuclei. Prog. Part. Nucl. Phys. **37**, 193–263 (1996). https://doi.org/10.1016/0146-6410(96)00054-3
40. J. Meng, H. Toki, S. Zhou et al., Relativistic continuum Hartree Bogoliubov theory for ground-state properties of exotic nuclei. Prog. Part. Nucl. Phys. **57**, 470–563 (2006). https://doi.org/10.1016/j.ppnp.2005.06.001
41. D. Vretenar, A. Afanasjev, G. Lalazissis et al., Relativistic Hartree–Bogoliubov theory: static and dynamic aspects of exotic nuclear structure. Phys. Rep. **409**, 101–259 (2005). https://doi.org/10.1016/j.physrep.2004.10.001
42. T. Nikšić, D. Vretenar, P. Ring, Relativistic nuclear energy density functionals: Mean-field and beyond. Prog. Part. Nucl. Phys. **66**, 519–548 (2011). https://doi.org/10.1016/j.ppnp.2011.01.055
43. J. Meng, J. Peng, S.Q. Zhang et al., Progress on tilted axis cranking covariant density functional theory for nuclear magnetic and antimagnetic rotation. Front. Phys. **8**, 55–79 (2013). https://doi.org/10.1007/s11467-013-0287-y
44. J. Meng, *Relativistic Density Functional for Nuclear Structure* (World Scientific, Singapore, 2015). https://doi.org/10.1142/9872
45. S. Shen, H. Liang, W.H. Long et al., Towards an ab initio covariant density functional theory for nuclear structure. Prog. Part. Nucl. Phys **109**, 103713 (2019). https://doi.org/10.1016/j.ppnp.2019.103713
46. M. Sharma, G. Lalazissis, P. Ring, Anomaly in the charge radii of Pb isotopes. Phys. Lett. B **317**, 9–13 (1993). https://doi.org/10.1016/0370-2693(93)91561-Z
47. S.G. Zhou, J. Meng, P. Ring, Spin symmetry in the antinucleon spectrum. Phys. Rev. Lett. **91**, 262501 (2003). https://doi.org/10.1103/PhysRevLett.91.262501
48. J. Li, J.X. Wei, J.N. Hu et al., Relativistic description of magnetic moments in nuclei with doubly closed shells plus or minus one nucleon. Phys. Rev. C **88**, 064307 (2013). https://doi.org/10.1103/PhysRevC.88.064307
49. J. Li, Y. Zhang, J. Yao et al., Magnetic moments of ^{33}Mg in the time-odd relativistic mean field approach. Sci. China G **52**, 1586–1592 (2009). https://doi.org/10.1007/s11433-009-0194-y
50. J. Zhao, T. Nikšić, D. Vretenar, Microscopic model for the collective enhancement of nuclear level densities. Phys. Rev. C **102**, 054606 (2020). https://doi.org/10.1103/PhysRevC.102.054606
51. W. Zhang, W. Gao, G.T. Zhang et al., Level density of odd—a nuclei at saddle point. Nucl. Sci. Tech. **34**, 124 (2023). https://doi.org/10.1007/s41365-023-01270-8
52. J.W. Negele, B.D. Serot, E. Vogt, et al., *The Relativistic Nuclear Many-Body Problem*, Vol. 57 (United States, 1986)
53. F. Williams, G. Chan, J. Huizenga, The significance of shell corrections in the parameterization of numerical state density calculations. Nucl. Phys. A **187**, 225–248 (1972). https://doi.org/10.1016/0375-9474(72)90576-3
54. T. Døssing, A. Jensen, Nuclear level densities with collective rotations included. Nucl. Phys. A **222**, 493–511 (1974). https://doi.org/10.1016/0375-9474(74)90334-0
55. S. Hilaire, S. Goriely, Global microscopic nuclear level densities within the HFB plus combinatorial method for practical applications. Nucl. Phys. A **779**, 63–81 (2006). https://doi.org/10.1016/j.nuclphysa.2006.08.014
56. R. Capote, M. Herman, P. Obložinský et al., RIPL: reference input parameter library for calculation of nuclear reactions and nuclear data evaluations. Nucl. Data Sheets **110**, 3107–3214 (2009). https://doi.org/10.1016/j.nds.2009.10.004. (**Special Issue on Nuclear Reaction Data**)
57. A. Koning, D. Rochman, Modern nuclear data evaluation with the Talys code system. Nucl. Data Sheets **113**, 2841–2934 (2012). https://doi.org/10.1016/j.nds.2012.11.002. (**Special Issue on Nuclear Reaction Data**)

58. A.C. Larsen, I.E. Ruud, A. Bürger et al., Transitional γ strength in cd isotopes. Phys. Rev. C **87**, 014319 (2013). https://doi.org/10.1103/PhysRevC.87.014319
59. M. Guttormsen, A. Bagheri, R. Chankova et al., Thermal properties and radiative strengths in ^{160,161,162}Dy. Phys. Rev. C **68**, 064306 (2003). https://doi.org/10.1103/PhysRevC.68.064306
60. W. Long, J. Meng, N.V. Giai et al., New effective interactions in relativistic mean field theory with nonlinear terms and density-dependent meson–nucleon coupling. Phys. Rev. C **69**, 034319 (2004). https://doi.org/10.1103/PhysRevC.69.034319
61. G. Lalazissis, S. Karatzikos, R. Fossion et al., The effective force NL^3 revisited. Phys. Lett. B **671**, 36–41 (2009). https://doi.org/10.1016/j.physletb.2008.11.070
62. T. Nikšić, N. Paar, D. Vretenar et al., Dirhb: a relativistic self-consistent mean-field framework for atomic nuclei. Comput. Phys. Commun. **185**, 1808–1821 (2014). https://doi.org/10.1016/j.cpc.2014.02.027
63. G.A. Lalazissis, T. Nikšić, D. Vretenar et al., New relativistic mean-field interaction with density-dependent meson–nucleon couplings. Phys. Rev. C **71**, 024312 (2005). https://doi.org/10.1103/PhysRevC.71.024312
64. E.V. Litvinova, A.V. Afanasjev, Dynamics of nuclear single-particle structure in covariant theory of particle-vibration coupling: From light to superheavy nuclei. Phys. Rev. C **84**, 014305 (2011). https://doi.org/10.1103/PhysRevC.84.014305
65. A.P.D. Ramirez, A.V. Voinov, S.M. Grimes et al., Nuclear level densities of ^{64,66}Zn from neutron evaporation. Phys. Rev. C **88**, 064324 (2013). https://doi.org/10.1103/PhysRevC.88.064324
66. R. Chankova, A. Schiller, U. Agvaanluvsan et al., Level densities and thermodynamical quantities of heated $^{93-98}$Mo isotopes. Phys. Rev. C **73**, 034311 (2006). https://doi.org/10.1103/PhysRevC.73.034311
67. N.U.H. Syed, M. Guttormsen, F. Ingebretsen et al., Level density and γ-decay properties of closed shell Pb nuclei. Phys. Rev. C **79**, 024316 (2009). https://doi.org/10.1103/PhysRevC.79.024316
68. E. Melby, M. Guttormsen, J. Rekstad et al., Thermal and electromagnetic properties of ^{166}Er and ^{167}Er. Phys. Rev. C **63**, 044309 (2001). https://doi.org/10.1103/PhysRevC.63.044309
69. A. Rahmatinejad, T.M. Shneidman, N.V. Antonenko et al., Collective enhancements in the level densities of Dy and Mo isotopes. Phys. Rev. C **101**, 054315 (2020). https://doi.org/10.1103/PhysRevC.101.054315
70. A.C. Larsen, R. Chankova, M. Guttormsen et al., Microcanonical entropies and radiative strength functions of ^{50,51}V. Phys. Rev. C **73**, 064301 (2006). https://doi.org/10.1103/PhysRevC.73.064301
71. E. Alhassan, D. Rochman, A. Vasiliev et al., Iterative Bayesian Monte Carlo for nuclear data evaluation. Nucl. Sci. Tech. **33**, 50 (2022). https://doi.org/10.1007/s41365-022-01034-w
72. H.K. Toft, A.C. Larsen, U. Agvaanluvsan et al., Level densities and γ-ray strength functions in sn isotopes. Phys. Rev. C **81**, 064311 (2010). https://doi.org/10.1103/PhysRevC.81.064311
73. U. Agvaanluvsan, A. Schiller, J.A. Becker et al., Level densities and γ-ray strength functions in ^{170,171,172}Yb. Phys. Rev. C **70**, 054611 (2004). https://doi.org/10.1103/PhysRevC.70.054611
74. A.P.D. Ramirez, A.V. Voinov, S.M. Grimes et al., Level density and mechanism of deuteron-induced reactions on ^{54,56,58} Fe. Phys. Rev. C **92**, 014303 (2015). https://doi.org/10.1103/PhysRevC.92.014303
75. B.M. Oginni, S.M. Grimes, A.V. Voinov et al., Test of level density models from reactions of ^{6}Li on ^{58}Fe and ^{7}Li on ^{57}Fe. Phys. Rev. C **80**, 034305 (2009). https://doi.org/10.1103/PhysRevC.80.034305